Comparative Medicine
Copyright 2021
by the American Association for Laboratory Animal Science

Vol 71, No 6
December 2021
Pages 1–9

Case Study

Degenerative Osteoarthropathy in Laboratory Housed *Xenopus (Silurana) tropicalis*

Mingyun Zhang,[1] Sabrina S Wilson,[2] Kerriann M Casey,[1] Paisley E Thomson,[3] Anne L Zlatow,[1] Valerie S Langlois,[3] and Sherril L Green[1,*]

In this case study, 15 adult laboratory *Xenopus (Silurana) tropicalis* (7 adult males and 8 adult females) were examined for nodular enlargements of the clawed digits (digits 0, I, II, and III) on the hind feet. Radiographs showed smoothly margined, rounded, peripherally mineralized lesions arising from the distal phalanges of digits 0-III with osteoproductive and osteolytic components in all frogs. Micro computed tomography (microCT) scans further revealed interphalangeal (IP), metacarpophalangeal (MCP), and metatarsophalangeal (MTP) joint osteoarthritis characterized by periarticular new bone formation, rounded mineral foci both peripherally and centrally within the joints, and more rarely, linear mineralization palmar/plantar to the joints in the flexor tendons. In the nonclawed digits, the shape of the distal phalanx was variably distorted and both subluxation and malangulation of IP joints were identified. Histologically, nodules corresponded to a peripheral rim of mature cortical bone surrounding central adipose tissue, scattered hematopoietic elements, and residual bone of the distal phalanx. Occasionally, the peripheral rim of cortical bone extended proximally to encompass the distal aspect of adjacent phalanx. MCP, MTP and IP joint spaces of most digits exhibited widespread osteoarthritis characterized by periarticular cartilaginous or osseous metaplasia, bony remodeling, and less frequently, granulomatous osteomyelitis. Nutritional analyses of the feed did not indicate imbalances nor were the lesions consistent with metabolic bone disease. The exact etiopathogenesis of these lesions is unknown; however, we hypothesize that the osteoarthritic changes are due to a combination of the frogs' mature age, the unique structure of the *Xenopus* spp. claw, genetics and biomechanical forces on the digits and distal phalanges of the hind feet.

Abbreviations: IP, interphalangeal joint; MCP, metacarpophalangeal; microCT, micro computed tomography; MTP, metatarsophalangeal; X. tropicalis, Xenopus tropicalis

DOI: 10.30802/AALAS-CM-21-000061

Xenopus spp. are a well-established model in biomedical research and are commonly used in the fields of embryology and vertebrate developmental biology, endocrinology, toxicology, cancer, and genomics.[1-3,5,10,11,13,16,17,19,20,22] In research laboratory environments, *X. tropicalis* are typically housed in either static or recirculating aquatic systems in water maintained at 25 to 28 °C, with a pH between 6.8 and 8.5, and a hardness between 100 and 300 mg/L $CaCo_3$.[7] Housing tanks range in size from 1 L or more, depending on the needs of the laboratory and the type and configuration of the housing system. Stocking density ranges from approximately 1-5 adult frogs/L per tank.[7] Laboratory *X. tropicalis* are commonly fed commercially available complete and balanced pelleted diets 3 times per week, or as appropriate for their different life stages.[7,18,21] With stringent husbandry and disease surveillance protocols in place, laboratory-reared and housed *Xenopus* spp. generally remain healthy well through adulthood and their prime egg-producing years and can live 10 y or longer in captivity.[7]

To date, most reports describing disease in laboratory or wild *Xenopus* spp. are attributed to infectious agents (bacterial, viral, or parasitic) and/or conditions related to water quality aberrations or pollutants.[7] Naturally occurring bone diseases due to nutritional appear to be rare in laboratory *Xenopus* spp., although they have been described in other frogs and amphibians.[6,12,23] Reports of other spontaneous skeletal diseases in laboratory *Xenopus* are particularly rare. One group[25] recently described axial skeletal deformities in genetically engineered and wild type laboratory *Xenopus* spp. Here we report spontaneously occurring appendicular skeletal degenerative osteoarthropathy with hindlimb distal phalangeal nodules (digits 0-III) in mature, laboratory *X. tropicalis*, as confirmed by radiography, computed tomography and histopathology.

Materials and Methods

Animal husbandry and clinical history. The adult frogs described in this report were reared and housed for the purpose of studying water pollutants and endocrine disruptors. This colony has been bred inhouse and maintained by the laboratory of the principal investigator (coauthor VL) for over 10 y. This colony was established from an approximately 10 y old colony

Received: 15 Jun 2021. Revision requested: 29 Jul 2021. Accepted: 19 Aug 2021.
[1]Department of Comparative Medicine, Stanford University School of Medicine, Stanford, California; [2]Diagnostic Imaging Service, William R. Pritchard Veterinary Medical Teaching Hospital, School of Veterinary Medicine, University of California-Davis, Davis, California; [3]Institut National de la Recherche Scientifique (INRS) - Centre Eau Terre Environnement, Quebec, QC, Canada
[*]Corresponding author. Email: sherril@stanford.edu

that was also bred inhouse and maintained at another institution; however, the origins of this founder colony are unknown. All studies were approved by the Institutional Animal Care and Use Committee.

From August 2017 through April 2019, approximately 40 adult male and 40 adult female frogs were housed in 15 L clear static tanks and stocked at a density of approximately 2 frogs/L (males and females in separate tanks). Tanks were filled with charcoal-filtered, dechlorinated tap water at a water temperature of 25.0 ± 1 °C, and a water pH of 7.0 to 8.0. Tank water was hand-changed by approximately 30% to 50%, 3 times per week, approximately 2 h after feeding. Tank water was verified to be chlorine free by active chlorine monitors through the KAPTA 2000 controller and KAPTA 2000-AC2 sensor systems (Veolia Water Technologies, Saint-Maurice, France). Water nitrite, nitrate, and ammonia levels were tested weekly using Nutrafin test kits (Hagen, Baie d'Urfé, QC, Canada) and parameters maintained within the following ranges: ammonia (0.00-0.5 mg/L), nitrate (0.00 to 50 mg/L), and nitrite (0.00-0.5 mg/L). The tanks were cleaned once a month with clean scouring pads. No detergents or other cleaning agents were used. From Aug 2017 through 2018, frogs were fed approximately 20 g per tank (3 pellets/female; 2 pellets/male) of Nasco frog brittle (Nasco, Ft. Atkinson, WI), once a day, 7 d per week.

In 2018, Nasco notified the laboratory that the company would no longer export frog brittle to Canada. In response, the laboratory transitioned the colony to Ward's Science frog feed (Ward's Science, West Henrietta, NY) by feeding a mixture (50/50 by weight) of Nasco frog brittle and Ward's Science frog feed from August 2018 through January 2020, providing the same quantity per frog and at the same frequency as described above. The frogs were fully transitioned to Ward's Science frog feed by February 2020. In April of 2020, this colony was relocated to a new institution and transitioned to a third diet, *Xenopus Express* frog food diet (*Xenopus Express*, Brooksville, FL). The colony has since remained on *Xenopus Express* frog diet. The incidence of the toe lesions has not changed since its peak in 2019, with approximately 33 of 65 (51%) of the adults in the colony affected over the course of feeding these different diets. The frogs were maintained in a 12-h light:dark cycle and health checks were performed daily by laboratory personnel. This cohort of frogs had no history of infectious diseases or parasites.

In April 2019, the laboratory relocated to another institution, and the frogs were transferred into a new static system that used RO water reconstituted with Ocean Salts (Instant Ocean Reef Salt, Instant Ocean Spectrum, Blacksburg, VA) and maintained at a pH of 7.0 to 8.0 with a conductivity of 1000 to 1200 µS, measured through Thermo Scientific ELITEPCTS pocket pH/conductivity meter (Hogentogler and CO., Columbia, MD). Water in the static system was exchanged by 50%, 3 times per week approximately 2-6 h after feeding. The stocking density and light/dark cycle remained as described above.

Laboratory personnel first noticed nodules on the distal end of the digits of the hind feet of an adult male frog in August 2017 (prior to the laboratory's relocation) and relayed this finding to one of the coauthors (SG). Aside from the nodules on the digits, the affected frog was otherwise healthy (fecund, swimming, eating as normal). By November 2019, 7 mo after the laboratory's relocation, the nodules of the initially affected male had enlarged. In addition, nodular lesions were seen on other adult frogs in this cohort (Figure 1 A through D). The laboratory reported that the number of affected frogs had increased to 51% (33 of 65 frogs). All affected frogs, estimated to be between 3 and 7 y of age, also remained in good health otherwise, could swim normally, continued to eat, maintained their body weight and condition and remained fecund. No nodules were observed on the digits of the front feet, although the digital nodules on the hind feet of all affected frogs became larger over time. Arrangements were made to ship carcasses of affected frogs to Stanford University's Veterinary Service Center for diagnostics. Based on the clinical history and gross appearance, initial differential diagnoses included infectious disease, gout, pseudogout, metabolic bone disease, and neoplasia.

In the spring of 2019, 15 affected frogs were humanely euthanized in buffered tricaine sulfate (MS222, Thermo–Fisher, Waltham, MA). Decapitation was performed after death as required by the home institution. The carcasses were transported on cold packs via international couriers to Stanford University for evaluation by radiographic and computed tomographic studies, necropsy and histopathology. In addition, feed samples were shipped via an overnight-courier to Stanford University Veterinary Diagnostic Laboratory, and subsequently sent to Cornerstone Laboratories (Cornerstone Laboratories, Memphis, TN) for nutritional analysis.

Diagnostic tests. ***Feed analysis*****.** Individual one-hundred-gram samples of Nasco frog brittle (Nasco, Ft. Atkinson, WI), a 50/50 mix by weight of Ward's Science frog feed and Nasco frog brittle, Ward's Science frog feed, and Xenopus Express frog food were collected from the laboratory's Xenopus food stock supply and analyzed at Cornerstone Laboratories. The components of the feed analysis included: crude protein, crude fat, crude fiber, total moisture, total ash, total carbohydrates, total gross energy, total calcium, total phosphorous, total potassium, total magnesium, total copper, vitamin D3 as cholecalciferol, vitamin C as L-Ascorbic Acid Phosphate, and vitamin A as retinyl acetate. Methods used to measure each component are defined by the Association of the Official Analytical Collaboration International.[8]

Radiography and MicroCT Imaging. Carcasses from 7 of 15 frogs described in this report were selected for imaging studies. The pelvic limbs of the carcasses of 2 frogs (1 male and 1 female) were radiographed using a Sedecal APR-VET generator (Sedecal Vet Ray Technology, Arlington Heights, IL) at 80 kVp and 3.5 mAs and a digital radiograph plate (Smart DR 1717G, Sound Technologies, Carlsbad, CA). Ventrodorsal, dorsoventral, and ventrodorsal oblique images of each affected pes were obtained. The pelvic limbs of 4 frogs (2 females and 2 males) and the pelvic and thoracic limbs of 3 additional frogs (females) underwent computed tomography at the Stanford Center for Innovation in In vivo Imaging (SCi3) (Small Animal Imaging Service Center, Stanford, CA) to further characterize the lesions on the digits. MicroCT scans were acquired with the Bruker SkyScan 1276 microCT at 40 kV and 200 µA with 21 µm image pixel size and rotation step of 0.4 degree in 360 degrees (Bruker BioSpin Corp, Billerica, MA). Images were reconstructed using the Bruker NRecon package with flat field correction and no filter. MicroCT images were evaluated using multiplanar reconstruction and 3D volume rendering with Horos (Horosproject.org, Nimble LLC d/b/a Purview, Annapolis, MD).

Necropsy and histopathology. Eight affected adult frogs (4 males and 4 females) were selected for necropsy and histopathology. Frogs were humanely euthanized by immersion in 0.5% MS222, followed by decapitation to ensure death. Skin was swabbed and samples were submitted to the Amphibian Disease Laboratory (San Diego Zoo Wildlife Alliance, San Diego, CA) for Batrachochytrium dendrobatidis detection via PCR. The coelomic cavity was opened with a ventral midline incision, from pubis to snout. A single affected digit from each

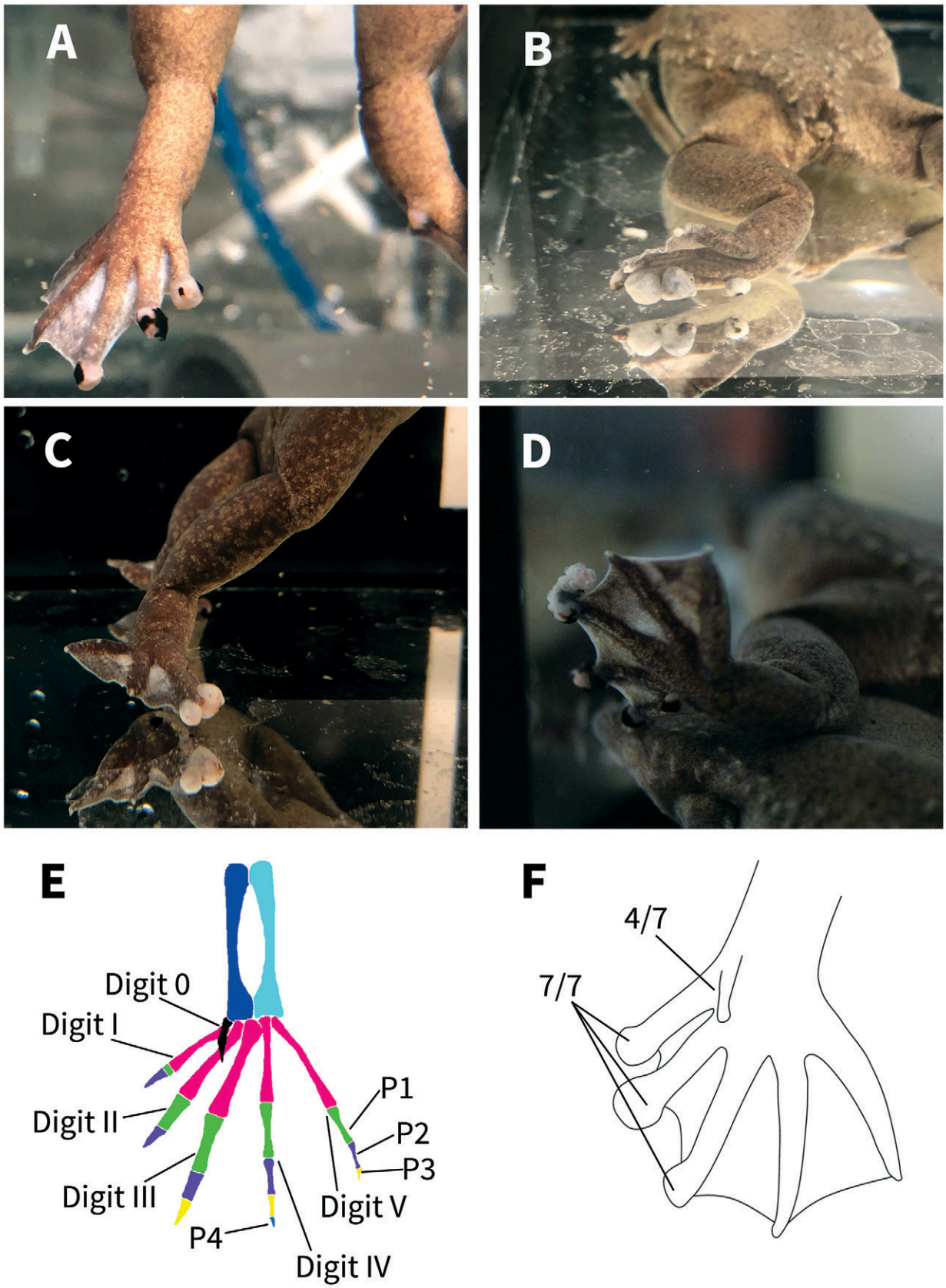

Figure 1. The gross figures of the feet of affected frogs. Four *X. tropicalis* displaying nodules on the distal aspects of the digits of the hindlimbs (A-D). The bone anatomy of a normal hindlimb (E). The normal *X. tropicalis* hind foot is characterized by: digit 0 shown in black, metatarsals in pink, tibiae in sky blue, fibulae in blue, first phalanx (P1) in green, second phalanx (P2) in purple, third phalanx (P3) in yellow, fourth phalanx (P4) in royal blue (on digit IV). Claws are only present on digits 0, I, II, and III. Note the normal, triangular-shaped distal phalanx. Hind foot diagram demonstrating which digits are the most affected (F). Seven frogs submitted directed to Stanford Necropsy Laboratory displayed nodules on the distal end of digits I, II, III of the hindlimbs. None of the frogs displayed nodules on digits IV or V.

frog was disarticulated and immersed in 100% ethanol for evaluation of urate tophi. The carcasses were then submerged in 10% neutral buffered formalin with a tissue to formalin ratio of 1:10 for at least 72 h. After fixation, wet tissues were sent to Antech Diagnostics Canada (Mississauga, Ontario, Canada) for gross dissection and routine tissue processing. Carpi and tarsi were disarticulated and decalcified in Cal-Ex II (Fischer Scientific, Upland, CA) prior to processing. Briefly, soft tissues (liver, kidneys, lung, heart, gastrointestinal tracts, and reproductive tracts) and decalcified bone sections were embedded in paraffin, sectioned at 4 µm, and stained with hematoxylin and eosin (H and E). Granulomatous bone lesions were stained with Grocott–Gomori's methenamine silver (GMS) and Ziehl–Neelsen (ZN) to evaluate for the presence of fungus and acid-fast bacteria, respectively. Tissues were also examined under compensated polarized light to evaluate for crystal birefringence. All slides were examined by board-certified veterinary pathologists.

Results

Imaging. Radiographs of the hind limbs from 2 X. tropicalis (1 male and 1 female) showed smoothly margined, rounded peripherally mineralized lesions arising from the distal phalanges of digits 0-III in both frogs (Figure 2). These lesions had osteoproductive and osteolytic components comprised of smoothly margined, bulbous to lobulated expansile periosteal new bone centered on the distal phalanx and variable lysis of the underlying phalanges. The more severely affected digits had extension of the expansile periosteal new bone and osteolysis proximally across the distal IP joint, involving the adjacent phalanx and distorting the distal IP joint articulation (Figure 2 B). The new bone extended as far proximally as the MTP joint in one pes. MicroCT (Figure 3 C) confirmed the radiographic findings, showing peripherally mineralized rounded lesions surrounding the distal phalanx of digits 0-III with retention of distorted and partially lysed distal phalanx centrally within the lesion. The expansile periosteal bone extended proximally to the level of the distal IP joint in the least affected digits and extended to the level of the MTP joint in the most affected digits (Figure 4). In addition to the nodular lesions, microCT further revealed that all frogs had IP, MCP and MTP joint osteoarthritis of variable severity characterized by periarticular new bone formation, rounded mineral foci both peripherally and centrally within the joints, and more rarely, linear mineralization palmar/plantar to the joints in the flexor tendons (Figure 4). In the nonclawed digits, the shape of the distal phalanx was variably distorted. Both subluxation and malangulation of IP joints were identified. However, expansile phalangeal lesions were not seen in the nonclawed digits.

MicroCT images also revealed that one frog had coxofemoral osteoarthritis, 2 frogs had cubital osteoarthritis, and 2 frogs had stifle joint osteoarthritis characterized by rounded mineral foci

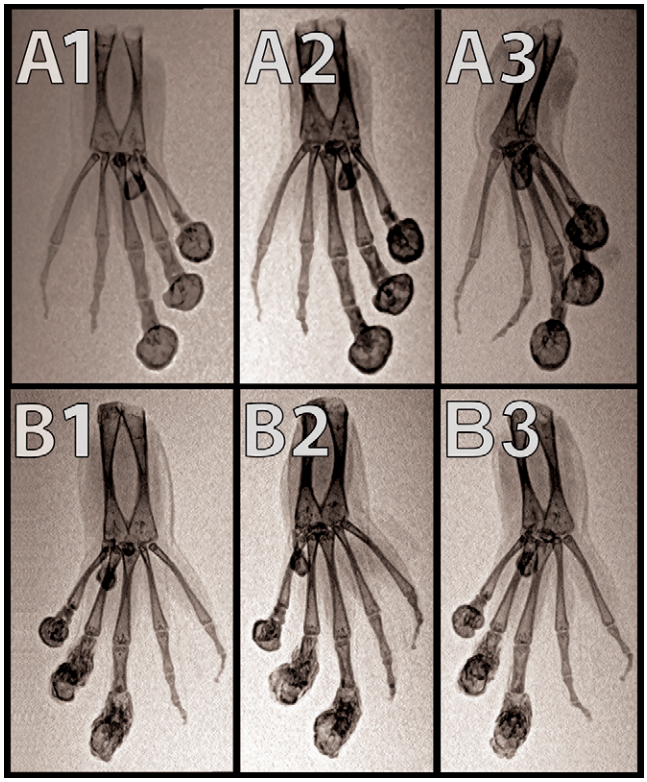

Figure 2. Dorsoventral (A1), ventrodorsal oblique (A2), and ventrodorsal (A3) inverted-grayscale radiographs of the left hindfoot. Dorsoventral (B1), ventrodorsal oblique (B2), ventrodorsal (B3) inverted-grayscale radiographs of the right hind foot of an affected *X. tropicalis*. Smoothly margined, rounded peripherally mineralized lesions are present on the distal aspects of digits 0, I, II, and III. Note the malangulation of P4 and P3 on digit IV. Note the malangulation of P3 and P2 on digit V.

Figure 3. Reconstructed dorsal plane CT image of a normal MTP and IP joint (A), reconstructed dorsal plane CT image of a severely affected MTP joint and IP joint (B) with periarticular new bone formation (asterisks *) and new bone formation within the joint space (daggers †), and reconstructed sagittal plane CT image of a severely affected digit (C) with a misshaped distal phalanx surrounded by a rim of new bone (arrowheads xxx) and linear mineralization plantar to the digit within the extensor tendons (NB).

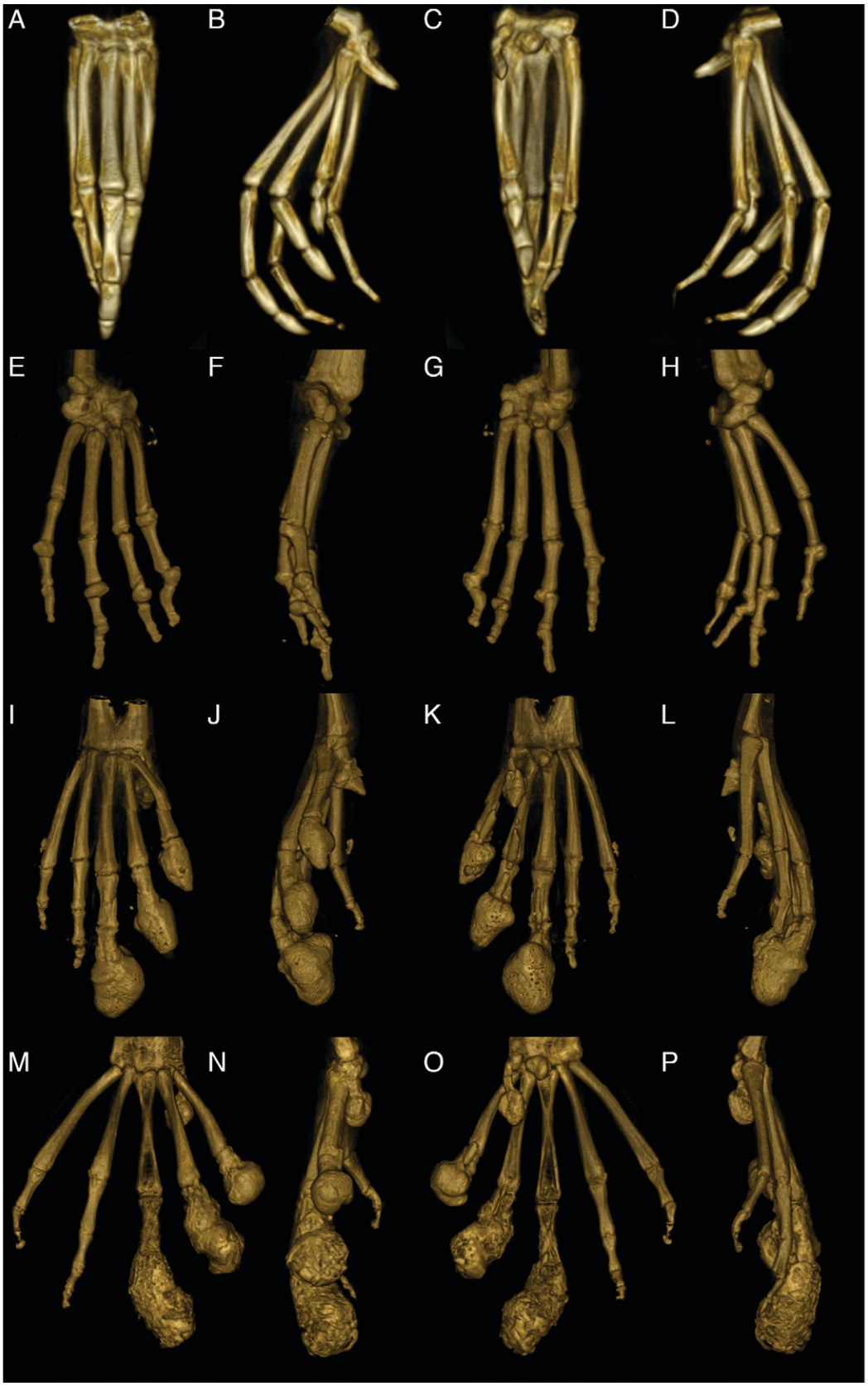

Figure 4. Reconstructed 3D volume renderings of a normal pes (A-D), a severely affected manus (E-H), a severely affected pes (I-L), and the most severely affected pes (M-P). A, E, I and M are dorsal views; B, F, J, and N are medial views, C, G, K, and O are palmar/plantar views, and D, H, L, and P are lateral views. A-D: Normal pes. E-H: Severely affected manus with severe periarticular and articular new bone formation in multiple MCP and IP joints with malangulation and subluxation of the IP joint. I-L: Severely affected pes that has rounded peripherally mineralized lesions on digits 0-III which extend proximal to the IP. There is severe linear mineralization plantar to digits I-IV in the flexor tendons. Similar to the manus, there is periarticular and articular new bone formation in the MTP and IP joints in the nonclawed digits and of the clawed digits proximal to the rounded lesions. M-P: Most severely affected pes with rounded peripherally mineralized lesions extending to the proximal phalanx, linear mineralization plantar to digits I-III, and severe periarticular new bone formation.

adjacent to the joints consistent with dystrophic mineralization of joint associated soft tissues. Osteoarthritic lesions were identified in the MTP, MCP, and IP joints of the forelimb and hindlimb digits in all frogs; proximal appendicular skeletal osteoarthritis was seen less commonly. One frog had a rotational deformity of the sacrum with unilateral malformation of the sacroiliac joint, as reported previously.[25]

Feed analyses and related calculations. Results obtained from feed analyses are shown in Figure 5. A consistent finding that would indicate a nutritional imbalance in the feed was not identified. The mixed diet was slightly higher in crude fat, total carbohydrate, total gross energy, and had a slightly lower Ca: P ratio, but the mixed feed values were otherwise consistent with other feeds evaluated. Ward's Science food had a higher crude fat, total carbohydrate, total gross energy, and slightly lower Ca: P ratio than the mixed diet that was fed during the transition.

Necropsy and histopathology. Eight adult, sexually mature frogs (4 males and 4 females) were submitted for necropsy examination. Grossly, smoothly contoured, firm, exophytic, 1 mm – 4 mm nodules were noted on the distal aspects of the digits. Nodules were mottled gray to brown to black. Frogs were affected to varying degrees with nodular lesions exclusively on the clawed digits (digits 0-III) (Figure 1 F). The claws were missing or were loosely attached on several digits. No other gross abnormalities were observed. Histologically, all frogs (8 of 8) exhibited some degree of phalangeal pathology in at least one clawed digit, regardless of gross appearance. A brief summary of gross and histologic findings can be found in Figure 6. No differences were seen between male and female frogs in the frequency, distribution, or character of the lesions. Nodular digital lesions (6 of 8 frogs) were composed of a moderately thick peripheral rim of mature, well-organized cortical bone that elevated the adjacent dermis and epidermis. The peripheral rim of cortical bone surrounded mature adipose tissue, scattered hematopoietic elements, and residual bone of the distal phalanx (Figure 7 A). The peripheral rim of cortical bone occasionally extended proximally to encompass the distal aspect of the adjacent phalanx. Myxedematous stroma occasionally surrounded the peripheral rim of cortical bone and was associated with low numbers of scattered macrophages, lymphocytes, and plasma cells.

In addition to nodular lesions, IP joint spaces were often incongruous and frequently contained nonrefractile, amorphous, mineralized deposits (Figure 7 B and D) and/or proliferative fibrocartilaginous tissue (Figure 7 B). Articular hyaline cartilage was occasionally eroded and often seen in conjunction with periosteal new bone formation, periarticular cartilaginous and osseous metaplasia, and general bony remodeling of the distal phalanges (Figure 7 D). Monosodium urate crystals in the tissues, which are an indicator of gout, were not observed.

In 3 of 8 frogs, the subcutis and adjacent malformed bone (typically the distal phalanx) were infiltrated by single or coalescing nodules of granulomatous inflammation, and rarely, multinucleated giant cells. Adjacent bone was often characterized by osteoclastic resorption and/or osteoblastic new bone formation. In 2 of the frogs, granulomatous inflammation surrounded islands of necrotic bone (bony sequestra). Neither GMS nor ZN staining identified any infectious organisms within

Component	Nasco*#	Mixed Diet	Canadian Ward's Science**	Xenopus *Express*™***	Reference Method
Crude Protein (%)	48.70%	47.50%	45.90%	47.70%	AOAC-992.23
Crude Fat (%)	4.90%	5.70%	8.20%	6.10%	AOAC-948.22
Crude Fiber (%)	2.50%	2.80%	2.70%	3.50%	AOAC-991.43
Total Moisture (%)	6.70%	6.40%	5.40%	8.30%	AOAC-935.29
Total Ash (%)	15.70%	11.90%	9.50%	9.50%	AOAC-920.48
Total Carbohydrates (%)	24.00%	29.00%	31.00%	25.00%	Calculation
Total Gross Energy (Kcal/kg)	2700Kcal/kg	2950Kcal/kg	3190Kcal/kg	2810Kcal/kg	Calculation
Total Calcium (%)	2.08%	1.99%	1.27%	1.50%	AOAC-984.27
Total Phosphorus (%)	1.75%	1.72%	1.10%	1.02%	USP-730
Total Calcium: Total Phosphorus %	119%	116%	115%	148%	Calculation
Total Potassium (%)	0.66%	0.62%	0.54%	0.39%	AOAC-984.27
Total Magnesium (%)	0.117%	0.125%	0.104%	0.100%	AOAC-984.27
Total Copper (ppm)	14ppm	10ppm	8ppm	10ppm	AOAC-984.27
Vitamin D as Cholecalciferol (IU/kg)	12400IU/kg	12800IU/kg	12000IU/kg	2320IU/kg	AOAC-2002.05 Modified
Vitamin C as Stay C (mg/100g)	2mg/100g	2.5mg/100g	1mg/100g	2.6mg/100g	EURL-1256378
Vitamin A as Retinyl Acetate (IU/kg)	1864.8IU/kg	1598.4IU/kg	1798.2IU/kg	12,154.5IU/kg	AOAC-2002.06

All feed stored in opaque airtight containers at room temperature (25.0 +/- 1 °C).

*This diet is frog brittles made for adult *Xenopus* spp.. This diet was fed until August 2018.

**This diet is Ward's Science food for adult *Xenopus* spp.. This diet was fed since February 2020 until April 2020.

*** This diet is Xenopus *Express*™ Premium sinking frog food (100% sinking). This diet was fed since April 2020.

#The lesion was first observed when feeding this diet.

Figure 5. Nutritional analysis of Nasco adult frog brittle, mix of Nasco adult frog brittle and Ward's Science frog brittle, Ward's Science frog brittle, and *Xenopus Express Xenopus* diet content. Analysis was performed by Cornerstone laboratories, LLC (Cornerstone Laboratories, LLC, Memphis, TN).

	Gross Distribution												Histopathology		
	Left Tarsus (Digits)						Right Tarsus (Digits)								
Frog ID	0	I	II	III	IV	V	0	I	II	III	IV	V	Interphalangeal Osteoarthritis	Nodular Distal Phalangeal Bone Growth	Granulomatous Osteomyelitis[a]
4	-	-	-	-	-	-	-	-	-	-	-	-	X	-	-
5	X	X	X	X	-	-	X	X	X	X	-	-	X	X	X
7	X	X	X	X	-	-	X	X	X	X	-	-	X	X	-
8	X	X	X	X	-	-	X	X	X	X	-	-	X	X	X
9	X	X	X	X	-	-	X	X	X	X	-	-	X	X	-
12	-	-	-	-	-	-	-	-	-	-	-	-	X	-	-
14	X	X	X	X	-	-	X	X	X	X	-	-	X	X	X
15	X	X	X	X	-	-	X	X	X	X	-	-	X	X	-

Figure 6. Gross distribution and histopathologic characteristics of phalangeal nodules in *Xenopus tropicalis*.

regions of inflammation. Skin swabs submitted for PCR testing for *Batrachochytrium dendrobatidis* were negative.

Histologically, hepatocytes were moderately to markedly expanded by micro- to macro-vesicular lipid vacuoles, and melanomacrophage aggregates were present, subjectively evaluated as higher in number and size in male frogs as compared with female frogs. All frogs exhibited mild tubular ectasia (dilation) with luminal mineralized deposits, mild lymphoplasmacytic interstitial nephritis, and periglomerular to interstitial fibrosis. The hepatic and renal findings summarized above were considered typical for aged laboratory *Xenopus* spp.

Discussion

The observation of multiple nodular lesions on the clawed digits (digits 0-III) of the hind feet of mature, adult, laboratory *Xenopus tropicalis* prompted this clinical investigation. Based on the frogs' signalment, clinical signs and clinical history, the initial differential diagnoses included metabolic bone disease, infectious disease, gout/pseudogout, or neoplasia. However, nutritional analysis of the diets revealed no imbalances, and the histologic lesions were not consistent with metabolic bone disease (for example, fibrous osteodystrophy, rickets, osteoporosis). *Batrachochytrium dendrobatidis* was not detected via PCR of tissue samples and no infectious agents were observed after special histologic staining. No histological evidence of neoplasia was found.

Radiographic findings and CT studies revealed smooth margined, rounded peripherally mineralized nodular lesions arising from the distal phalanges, digits 0-III, with osteoproductive and osteolytic components centered on the distal phalanx. Variable lysis of the underlying phalanges, and osteoarthritis was identified in the MTP, MCP, and IP joints, and less commonly in the proximal appendicular skeleton. The nonclawed distal phalanges of the manus and pes were often misshapen with joint subluxation. Histologically, nodular lesions were characterized by a peripheral rim of cortical bone surrounding residual fragments of the distal phalanx, mature adipose tissue, and scattered hematopoietic elements. Occasionally, the rim of cortical bone extended proximal to the distal IP joint to the distal aspect of the adjacent phalanx. Taken together, these lesions represent the first time degenerative osteoarthropathy has been documented in laboratory housed *X. tropicalis*.

The development of the nodular lesions on distal phalanx of tarsal digits 0-III and the subsequent phalangeal osteoarthritis are presumed to reflect a reactive process in the face of anatomic changes of both IP joints and claw attachments to the distal phalanx. In the digits without claws, IP joint subluxation and malalignment were seen concurrent with osteoarthritis; however, the nodular lesions were not seen. The nodules lacked the histologic features of reactive callus and periosteal new bone formation. The bilateral nature and exclusive anatomic distribution of the phalangeal nodules to the clawed digits 0-III on the hind feet suggest that biomechanical forces related to weight-bearing may underlie lesion development. *Xenopus* spp. normally use their hind feet to propel themselves off of solid surfaces in the tank and frequently rest on their hind feet with the claws in contact with the bottom surface of the tank. As these frogs aged, weight-bearing and biomechanical forces related to this behavior may have contributed to the formation of these nodular lesions. These lesions have not been reported in wild *Xenopus* spp. However, the natural habitat of *Xenopus* spp. includes small bodies of water, the resting areas of which are generally soft and muddy,[7] cushioning the biomechanical forces on the hindlimbs and the joints. In addition, the anatomic interaction of P3 with the overlying dermis, keratinocytes and mechanism of claw growth, attachment and formation in *Xenopus* spp. may play a role in the development of this lesion.[14,15] The pattern of *Xenopus* spp. claw sheath growth is distinct from other species.[4,9,14,15] Claw sheaths of *Xenopus* spp. are formed by corneocytes at the distal tips of the digits, with successive layers arising underneath the first layer and extending proximally. This allows the sheath to grow along its entire length and in a unique vertical growth pattern.[14] Repetitive mechanical forces on the distal tips of the *Xenopus* spp. claw may interrupt this growth pattern, resulting in the reactive, boney nodular lesions on digits 0-III, as described in this report. Although nail growth and attachment anatomy is different in humans, trauma to the nail bed and osteoarthritis in humans are also known to alter nail shape.[4] Notably, the arthritic lesions in the joints are not grossly apparent and therefore signs of the condition are not recognizable until the gross lesions at the end of the digits appear. We believe the nodular lesions on the distal phalanges appear later in the osteodegenerative process; testing this hypothesis would require serial imaging of multiple frogs as they age.

Given the number of frogs affected in this inhouse colony of *X. tropicalis*, a colony that has been maintained for more than a decade and that has produced many generations of frogs, one possibility is that this particular cohort of frogs has developed

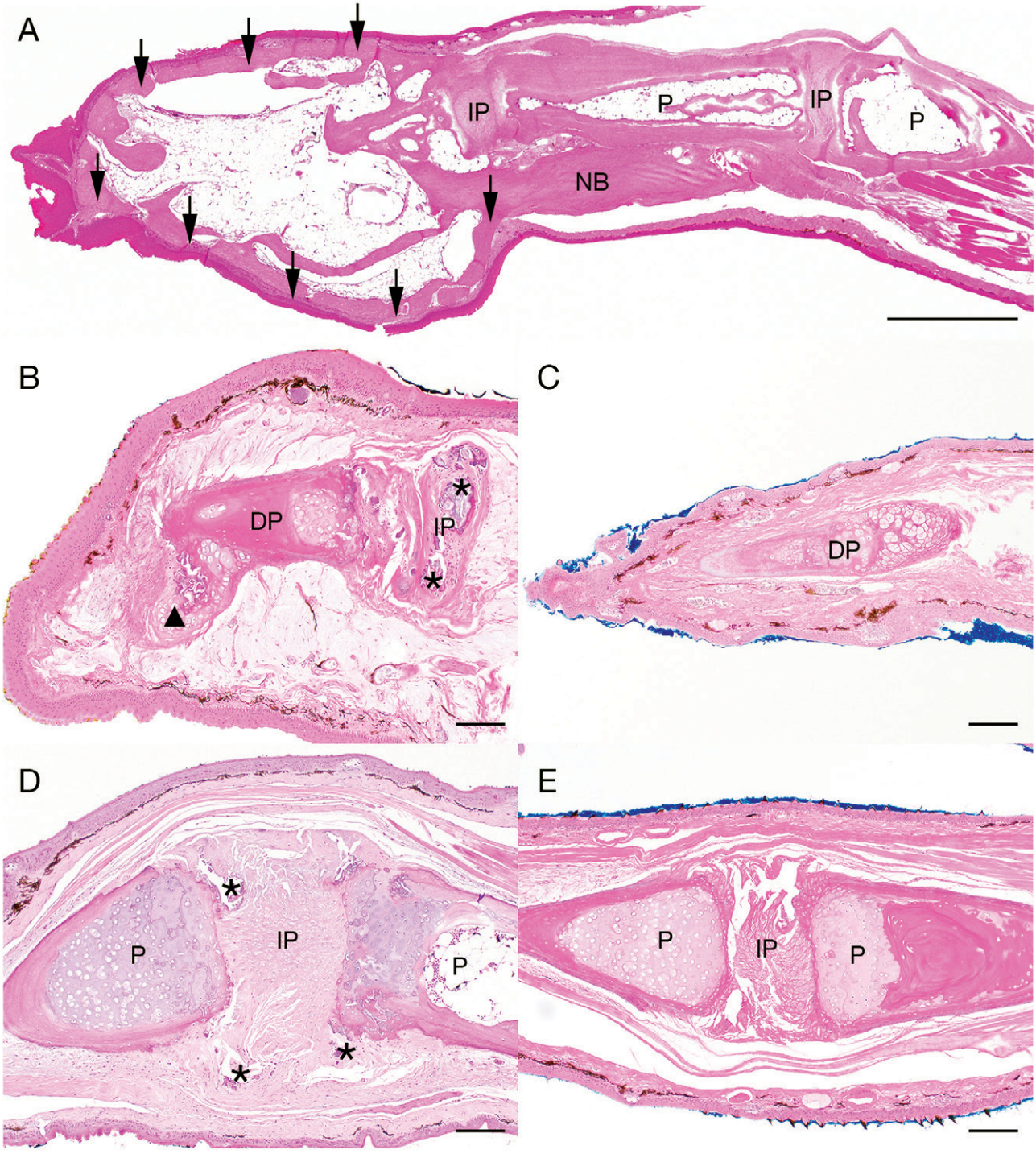

Figure 7. Histologic lesions in tarsal digits 0, I, II, and III of *Xenopus tropicalis*. Sagittal section of affected tarsal digit III (A). Nodular lesions comprised a peripheral rim of cortical bone (black arrows ↓) that occasionally extended proximally to form a layer of new bone (NB) surrounding preexisting bone of the adjacent phalanx (P). Centrally, the nodule was composed of mature adipose tissue and scattered hematopoietic elements. H and E, scale bar = 1 mm. Bony remodeling of the distal phalanx and IP osteoarthritis (B). The distal phalanx (DP) is irregularly contoured with fibrocartilaginous metaplasia extending from the distal aspect (arrowhead xxx). Myxedematous stroma surrounds the DP. The IP joint space contains abundant mineral (asterisks *). Note: The adjacent phalanx is out of the plane of section. H and E, scale bar = 100 µm. Unaffected DP (C). H and E, scale bar = 100 µm. An affected IP joint space exhibiting incongruity of adjacent phalanges (P) with IP mineralization (asterisks *) (D). H and E, scale bar = 100 µm. Normal adjacent phalanges, IP joint space (E). H and E, scale bar = 100 µm.

a genetic predisposition for this condition. Other epigenetic factors could also play a role. While thousands of *X. tropicalis* are used for research around the world, the prevalence of this condition in overall is unknown. However, the condition was been recently reported in a 7-y-old *X. tropicalis* at Stanford University in a colony that is presumably not related to this one.[24]

In summary, this is the first report of degenerative osteoarthropathy and osteoarthritis in laboratory *X. tropicalis*. Nodular phalangeal lesions on the hindlimb digits 0-III, osteoarthritis in the MCP, MTP, and IP joints of the forelimbs and hindlimbs, and rare lesions in the proximal appendicular skeleton were characterized by microCT and histopathologic evaluation.

While the exact etiopathogenesis is unknown, the authors propose that several factors may be involved, including age, genetics, biomechanical forces on the hindfeet and limbs of this semiaquatic species, and its unique mechanism of claw sheath growth and attachment. While the digital nodules enlarged over time, the animals' mobility and ability to feed did not appear to be compromised and affected frogs maintained body weight comparable to that of their unaffected cohorts. However, continuous monitoring of the affected frogs, by veterinary and caretaking staff is recommended.

Acknowledgments

The authors thank the Small Animal Imaging Facility, Stanford Center for Innovation and In-Vivo Imaging, VSC Animal Diagnostic Laboratory and Animal Histology Services, Department of Comparative Medicine, Stanford University, Jason Lee, Laura Pisani, Greg Nelson, RVT, and Elias Godoy for their assistance with our clinical and imaging investigations. We thank Janis Atuk-Jones for her technical and editing help with the article.

References

1. **Bissegger S, Langlois VS.** 2016. Androgens modulate gene expression and specific DNA methylation pattern of steroid 5□-reductases in the frog *Silurana tropicalis.* Gen Comp Endocrinol **234:**123–132. https://doi.org/10.1016/j.ygcen.2016.03.021.
2. **Campbell DE, Langlois VS.** 2018. Expression of sf1 and dax-1 are regulated by thyroid hormones and androgens during *Silurana tropicalis* early development. Gen Comp Endocrinol **259:**34–44. https://doi.org/10.1016/j.ygcen.2017.10.017.
3. **Chu C-W, Masak G, Yang J, Davidson LA.** 2020. From biomechanics to mechanobiology: *Xenopus* provides direct access to the physical principles that shape the embryo. Curr Opin Genet Dev **63:**71–77. https://doi.org/10.1016/j.gde.2020.05.011.
4. **de Berker D.** 2013. Nail anatomy. Clin Dermatol **31:**509–515. https://doi.org/10.1016/j.clindermatol.2013.06.006.
5. **Dumont JN.** 1972. Oogenesis in *Xenopus laevis* (Daudin). I. Stages of oocyte development in laboratory maintained animals. J Morphol **136:**153–179. https://doi.org/10.1002/jmor.1051360203.
6. **Ferrie GM, Alford VC, Atkinson J, Baitchman E, Barber D, Blaner WS, Crawshaw G, Daneault A, Dierenfeld E, Finke M, Fleming G, Gagliardo R, Hoffman EA, Karasov W, Klasing K, Koutsos E, Lankton J, Lavin SR, Lentini A, Livingston S, Lock B, Mason T, McComb A, Morris C, Perssier AP, Olea-Popelka F, Probst T, Rodriguez C, Schad K, Semmen K, Sincage J, Stamper MA, Steinmetz J, Sullivan K, Terrell S, Wertan N, Wheaton CJ, Wilson B, Valdes EV.** 2014. Nutrition and health in amphibian husbandry. Zoo Biol **33:**485–501. https://doi.org/10.1002/zoo.21180.
7. **Green SL.** 2009. The laboratory *Xenopus* sp. Boca Raton (FL): CRC Press.
8. **Horwitz W, Chichilo P, Reynolds H.** 1970. Official methods of analysis of the association of official analytical chemists. Washington: Assoc. of Official Analytical Chemists.
9. **Jäger K, Fischer H, Tschachler E, Eckhart L.** 2007. Terminal differentiation of nail matrix keratinocytes involves up-regulation of DNase1L2 but is independent of caspase-14 expression. Differentiation **75:**939–946. https://doi.org/10.1111/j.1432-0436.2007.00183.x.
10. **Kakebeen A, Wills A.** 2019. Advancing genetic and genomic technologies deepen the pool for discovery in *Xenopus tropicalis.* Dev Dyn **248:**620–625. https://doi.org/10.1002/dvdy.80.
11. **Keller R.** 1991. Early embryonic development of *Xenopus laevis.* Methods Cell Biol **36:**61–113. https://doi.org/10.1016/S0091-679X(08)60273-3.
12. **Klaphake E.** 2010. A fresh look at metabolic bone diseases in reptiles and amphibians. Vet Clin North Am Exot Anim Pract **13:**375–392. https://doi.org/10.1016/j.cvex.2010.05.007.
13. **Kobel HR, Du Pasquier L.** 1986. Genetics of polyploid *Xenopus.* Trends Genet **2:**310–315. https://doi.org/10.1016/0168-9525(86)90286-6.
14. **Maddin HC, Eckhart L, Jaeger K, Russell AP, Ghannadan M.** 2009. The anatomy and development of the claws of *Xenopus laevis (Lissamphibia: Anura)* reveal alternate pathways of structural evolution in the integument of tetrapods. J Anat **214:**607–619. https://doi.org/10.1111/j.1469-7580.2009.01052.x.
15. **Maddin HC, Musat-Marcu S, Reisz RR.** 2007. Histological microstructure of the claws of the African clawed frog, *Xenopus laevis (Anura: Pipidae)*: implications for the evolution of claws in tetrapods. J Exp Zool Part B Mol Dev Evol **308B:**259–268. https://doi.org/10.1002/jez.b.21145.
16. **Maia LA, Velloso I, Abreu JG.** 2017. Advances in the use of *Xenopus* for successful drug screening. Expert Opin Drug Discov **12:**1153–1159. https://doi.org/10.1080/17460441.2017.1367281.
17. **Mathieu-Denoncourt J, Martyniuk CJ, Loughery JR, Yargeau V, de Solla SR, Langlois VS.** 2016. Lethal and sublethal effects of phthalate diesters in *Silurana tropicalis* larvae. Environ Toxicol Chem **35:**2511–2522. https://doi.org/10.1002/etc.3413.
18. **McNamara S, Wlizla M, Horb ME.** 2018. Husbandry, general care, and transportation of *Xenopus laevis* and *Xenopus tropicalis*, p. 1-17. In: Vleminckx K editor. Xenopus Methods in Molecular Biology, vol 1865. Humana Press, New York, NY.
19. **Naert T, Vleminckx K.** 2018. Cancer models in *Xenopus tropicalis* by CRISPR/Cas9 mediated knockout of tumor suppressors. Methods Mol Biol **1865:**147–161. https://doi.org/10.1007/978-1-4939-8784-9_11.
20. **Rupp RA, Snider L, Weintraub H.** 1994. *Xenopus* embryos regulate the nuclear localization of XMyoD. Genes Dev **8:**1311–1323. https://doi.org/10.1101/gad.8.11.1311.
21. **Schultz TW, Dawson DA.** 2003. Housing and husbandry of *Xenopus* for oocyte production. Lab Anim (NY) **32:**34–39. https://doi.org/10.1038/laban0203-34.
22. **Tanaka M, Kuriyama S, Itoh G, Kohyama A, Iwabuchi Y, Shibata H, Yashiro M, Aiba N.** 2016. Identification of anti-cancer chemical compounds using *Xenopus* embryos. Cancer Sci **107:**803–811. https://doi.org/10.1111/cas.12940.
23. **Uhl EW.** 2018. The pathology of vitamin D deficiency in domesticated animals: an evolutionary and comparative overview. Int J Paleopathol **23:**100–109. https://doi.org/10.1016/j.ijpp.2018.03.001.
24. **Zhang M, Wilson S, Casey KM, Thomson P, Green SL.** 2021. The use of micro-computerized tomography as a diagnostic imaging aid investigating nodular lesions on the distal phalanges of the hindlimb in *Xenopus tropicalis*. 72nd AALAS National Meeting, Kansas City, Missouri, 17-21 October 2021. In press.
25. **Zlatow AL, Wilson SS, Bouley DM, Tetens-Woodring J, Buchholz DR, Green SL.** 2020. Axial skeletal malformations in genetically modified *Xenopus laevis* and *Xenopus tropicalis.* Comp Med **70:**532–541. https://doi.org/10.30802/AALAS-CM-20-000069.